A model for the residence time distribution of bubble-train flow in a square mini-channel based on direct numerical simulation results

Martin Wörner*, Bradut Ghidersa, Alexandru Onea

Forschungszentrum Karlsruhe, Institut für Reaktorsicherheit, Postfach 3640, 76021 Karlsruhe, Germany

Abstract

This paper presents an original method for evaluating the liquid phase residence time distribution in bubble-train flow using data from direct numerical simulations. The method is a particle method and relies on the uniform introduction of virtual particles in the volume occupied by the liquid phase within a single flow unit cell. The residence time distribution is obtained by statistical evaluation of the time needed by any particle to travel an axial distance equivalent to the length of the flow unit cell. Residence time curves are evaluated from DNS data of bubble-train flow in a square mini-channel for different lengths of the flow unit cell. The curves obtained are well fitted by an exponential relationship, which has been developed on basis of a two-tanks-in-series compartment model, where the first tank is a plug flow reactor and the second is a continuous stirred tank reactor.

Keywords: Bubble-train flow; Taylor flow; Residence time distribution; Direct numerical simulation

1. Introduction

Bubble-train flow (BTF) is a common flow pattern for gas-liquid flows in narrow channels. It consists of a regular sequence of bubbles of identical shape, which fill almost the entire channel cross-section and are often called Taylor bubbles. The individual bubbles are separated by liquid slugs and move with the same axial velocity. Therefore, bubble-train flow or Taylor flow is fully described by a single flow unit cell, which consists of one bubble and the liquid slug separating it from the trailing bubble. BTF is of considerable technical relevance, e.g. for monolithic reactors (Boger et al., 2004; Kreutzer et al., 2005a, 2005b) and for miniaturized multiphase reactors (Burns and Ramshaw, 2001; Hessel et al., 2004, 2005).

An important characteristic of any chemical reactor is its residence time distribution (RTD), since the RTD provides information about the flow and mixing behaviour of reaction components. In practice, the residence time distribution is often measured by a stimulus-response technique, where a specific quantity of tracer (e.g. fluorescent substance, radionuclide, solution of salt, etc.) is introduced at the system inlet as a short duration pulse or a step function and where the time variation of the tracer concentration at the outlet is recorded.

* Tel.: +49 7247 822577; fax: +49 7247 823718
E-mail address: woerner@irs.fzk.de

The tracer particles injected at the inlet are assumed to follow the same paths through the system as did the original fluid particles they replaced (Naumann, 1981). Thus, the tracer particles will have the same distribution of residence times as the original fluid particles. By recording the times when particles leave, a histogram can be constructed which, with a large sampling size, will converge to the differential residence time distribution function, $E(t)$. The probability that a particle had a residence time less than t is then given by the cumulative residence time distribution function

$$F(t) = \int_0^t E(t')\mathrm{d}t' \tag{1}$$

The extension of the above measurement principle from single phase flow to gas-liquid two phase flow presents no special difficulties (Naumann, 1981). The main difference is that the system has now usually two inlets (one for the gas phase and one for the liquid phase), while there is still one common outlet. To measure the residence time distribution of the liquid phase, the tracer pulse is injected at the liquid inlet only. For bubble-train flow, a measurement of the residence time distribution of the gas phase is not of interest, since the RTD is very narrow and its mean value can easily be computed from the travelling distance and the bubble velocity.

The stimulus-response measurement technique is well suited for macro-reactors, where the reactor volume is much larger than the volume of the tracer measuring unit. However, for micro-reactors the reactor volume is usually smaller than the volume of the measuring unit. This means that the residence time response of the tracer may already be influenced by the measuring construction itself (M. Günther et al., 2004). Measurements of liquid phase RTD for two-phase flow through narrow channels are reported by Thulasidas et al. (1999) for bubble-train flow in single straight channels, by Patrick et al. (1995) for a monolith froth reactor, by Heibel et al. (2005) for film flow in a monolith reactor, by Yawalkar et al. (2005) and Kreutzer et al. (2005a) for bubble-train flow in a monolith reactor, and by A. Günther et al. (2004) and Trachsel et al. (2005) for bubble-train flow in micro-fluidic channel networks of rectangular cross-section. The latter authors showed a narrow residence time distribution for bubble-train flow as compared to single phase flow.

An alternative way to determine the RTD is by means of computational fluid dynamics (CFD). There exist in principle two options to determine the residence time distribution from CFD methods (Thyn and Zitny, 2004). The first one is to numerically simulate the stimulus-response experiment, i.e. setting a short concentration pulse at the inlet of the computational domain, computing the unsteady concentration field of the tracer within the computational domain and evaluating it at the outlet. This approach has been used in a modified form by Salman et al. (2005) to determine the reactor residence time for Taylor flow in a circular microchannel from the residence time distribution of a single unit cell by using a convolution procedure. The second possibility is the particle tracking method. Here, virtual particles are released at the inlet and their trajectories are computed from the known velocity field of the CFD calculation (see e.g. Castelain et al., 2000). A notable difference between the two methods is that in the particle method only convective properties of the flow are monitored, while by evaluation of the unsteady concentration field additionally diffusive transport is taken into account. The relative importance of convective and diffusive transport is characterized by the Bodenstein number. For bubble-train flow, it can be defined as $Bo = U_B d_h / D_{tracer}$, where U_B is the bubble velocity, d_h is the hydraulic diameter of the channel and D_{tracer} is the molecular diffusion coefficient of the tracer in the liquid phase. For a particle

method, no diffusion of the tracer is taken into account. The RTD obtained by a particle method is therefore representative for an infinite value of the Bodenstein number.

To predict the residence time distribution for Taylor flow, Salman et al. (2004) developed a numerical model valid for low values of the Bodenstein number. This model assumes well mixed liquid slugs of uniform concentration and liquid films around the bubble that can be adequately described by a one-dimensional convection-diffusion equation. For large values of the Bodenstein number ($Bo > 10$) the model can be simplified to yield an analytical solution which corresponds to the representation of a unit cell by a tank-in-series model, consisting of a plug flow reactor (PFR) and a continuous stirred tank reactor (CSTR).

An important issue for measurement of the RTD or its computation by CFD is the introduction of the tracer at the inlet and its detection at the outlet, because this may strongly influence the obtained residence time distribution (Levenspiel and Turner, 1970; Levenspiel et al. 1970; Levenspiel, 1999). There are essentially two different concepts, namely the flux and planar introduction and measurement, respectively. Both approaches lead to different response curves which may, for laminar flow in a pipe or plane channel, be transformed into each other, see section 3.2.1. However, only the flux-flux method yields the proper RTD for reactor purposes (Levenspiel, 1999).

In this paper we present an original CFD-based method for evaluation of the residence time distribution of the continuous phase in bubble-train flow. Our method is a particle method and relies on the known bubble shape and velocity field within a unit cell, which are assumed to be available from direct numerical simulation (DNS). Particle methods are usually based on the computed *steady* velocity field. For BTF the velocity field is *unsteady* in the fixed frame of reference, for which the RTD has to be computed. It is, however, steady in the frame of reference moving with the bubble. In our method we take advantage of this fact and apply an appropriate transformation between the two frames of reference. Because the concept of planar introduction is not suited for BTF, we extend it to a volumetric introduction, where virtual particles are introduced in all mesh cells within the flow domain that are entirely filled with liquid. For each particle we determine the time the particle needs to travel an axial distance equal to the unit cell length. By appropriate weighting and normalization of the residence times of all particles, the residence time distribution is obtained.

The remainder of this paper is organized as follows. In section 2 we present direct numerical simulation results of co-current upward bubble-train flow of air bubbles through silicon oil in a square vertical channel of 2 mm × 2 mm cross section. In section 3 we introduce our original particle method for evaluation of the RTD in bubble-train flow. In section 4 we present results for the liquid phase residence time distribution in bubble-train flow and develop a model for the RTD obtained. Finally, we give conclusions and outlook in section 5.

2. Direct numerical simulation of bubble-train flow

In this section we first give a short overview on the numerical method and the computer code used to perform the direct numerical simulations of bubble-train flow. We then give the physical and numerical parameters of the simulations and provide a verification and discussion of the DNS results.

2.1. Numerical method

The direct numerical simulations are performed with the in-house computer code TURBIT-VOF, which solves the single-field Navier-Stokes equations with surface tension term for two incompressible immiscible fluids under assumption of constant fluid properties (i.e. density, viscosity, surface tension). The single-field formulation automatically accounts for the proper momentum jump conditions across the gas-liquid interface. The governing equations are written in non-dimensional form, see Ghidersa et al. (2004). For normalisation, a reference length scale L_{ref} and reference velocity scale U_{ref} are used, which need to be specified. The solution strategy is based on a projection method, where the resulting Poisson equation for the pressure is solved by a conjugate gradient solver. Time integration of the single field Navier-Stokes equation is done by an explicit third order Runge-Kutta method. Discretization in space is based on a finite volume method, where a regular Cartesian staggered grid is used. All derivatives in space are approximated by second order central differences.

For computing the evolution of the deformable interface which separates the two immiscible fluids, the volume-of-fluid (VOF) method is used. In any mesh cell that instantaneously contains both phases, the interface is locally approximated by a plane. The orientation and location of the plane is reconstructed from the discrete distribution of the volumetric fraction f of the continuous fluid. Note that - for a certain instant in time - we have $f = 1$ for mesh cells entirely filled with liquid, $f = 0$ for mesh cells entirely filled with gas, and $0 < f < 1$ for mesh cells that contain both phases. The evolution of f is governed by an advection equation, which expresses the mass conservation of the continuous phase. To avoid any smearing of the interface, this f-equation is not solved by a difference scheme. Instead, the flux of f across the faces of any interface mesh cell is calculated in a geometrical manner, depending on the location and orientation of the plane representing the interface. For further details about the numerical method we refer to Sabisch et al. (2001).

2.2. Simulation parameters

We now give a short overview on the simulations of bubble-train flow that we will use to analyse the RTD. The concept of the simulations is essentially the same as in a previous paper (Ghidersa et al., 2004). We consider one flow unit cell only and use periodic boundary conditions in vertical axial direction (y); see Figure 1 for a sketch of the computational domain and the co-ordinate system. The use of periodic boundary conditions in axial direction requires a special treatment of the pressure term. For this purpose a “reduced pressure” is defined, see Ghidersa et al. (2004). This reduced pressure is periodic because it does not involve the hydrostatic contribution and that of the linear axial pressure drop. As a result of this pressure decomposition, the buoyancy force and the axial pressure gradient appear as source terms in the Navier-Stokes equation. The simulations aim to reproduce the conditions of an experiment by Thulasidas et al. (1995), where the co-current upward flow of air bubbles in silicon oil of various viscosities in a square vertical channel with a cross section of 2 mm × 2 mm is investigated. This flow configuration was recently investigated numerically by Taha and Cui (2006) using the VOF method as implemented in the commercial CFD code FLUENT. The latter authors did, however, not consider bubble-train flow, but computed the flow of a single Taylor bubble and used inflow and outflow boundary conditions.

In Ghidersa et al. (2004) we presented simulations with a cubic flow unit cell for silicon oil of two different viscosities, which result in different values of the capillary number $Ca \equiv \mu_{\mathrm{L}} U_{\mathrm{B}}/\sigma$, namely $Ca \approx 0.04$ and $Ca \approx 0.2$. The capillary number is the relevant non-dimensional group for two-phase flow in narrow channels, as it represents the ratio of the two

dominant forces, namely viscous forces and surface tension. The influence of the capillary number is discussed in Ghidersa et al. (2004) and Taha and Cui (2006). In the present paper, we consider only the more viscous case, i.e. that one with higher value of *Ca*, where μ_L = 0.048 Pa s and ρ_L = 957 kg/m^3. While these values for the liquid density and liquid viscosity and the value for the coefficient of surface tension σ = 0.02218 N/m correspond to the experiment of Thulasidas et al. (1995), we increased in Ghidersa et al. (2004) the gas density and gas viscosity by a factor of 10 to improve the computational efficiency. So we used ρ_G = 11.7 kg/m^3 and $\mu_G = 1.84 \times 10^{-4}$ Pa s, which results in a liquid-to-gas density ratio of about 81 and a liquid-to-gas viscosity ratio of about 260. To investigate the effect of this artificial increase of ρ_G and μ_G we present, for comparison, in this paper one simulation for the real air properties, namely ρ_G = 1.17 kg/m^3 and $\mu_G = 1.84 \times 10^{-5}$ Pa s. In addition, a grid refinement study is performed for the case with increased gas density and viscosity to assess the influence of the mesh size.

As initial condition we place (for the simulations with a cubic unit cell only) a spherical bubble in the centre of the computational domain and start the simulations from fluid at rest. The diameter of the bubble is chosen so that the gas volumetric fraction in the unit cell ε is about 33%. In this paper we use for all simulations as reference length scale L_{ref} = 0.002 m (i.e. the width of the square channel in the experiment of Thulasidas et al. (1995)) and as reference velocity scale U_{ref} = 0.0264 m/s. The reference time scale then becomes $t_{ref} = L_{ref} / U_{ref}$ = 0.757 s. The driving axial pressure drop corresponds to a reference Euler number $Eu_{ref} \equiv |\Delta p_{Lref}| / (\rho_L U_{ref}^2) = 27$, where $|\Delta p_{Lref}|$ is the axial pressure drop per reference length. In Table 1 we list the time step width and number of time steps computed. As can be seen, the time step for case A1 is ten times smaller than for case A2 with increased gas density. In Figure 2 we show the temporal evolution of the bubble velocity and the mean velocity of the liquid phase. We see that the curves for cases A1, A2 and A3 show only very small differences. Figure 3 shows the temporal evolution of the bubble dimensions in the two wall-normal directions *x* and *z*. These bubble dimensions are computed as follows. For each mesh cell that contains both phases ($0 < f < 1$) the centroid of the plane representing the interface is computed. The centroids of neighbouring mesh cells are then connected to form triangles or quadrangles. This yields the closed bubble surface as shown in Figure 1 and Figure 5. By this procedure it is possible to determine the bubble dimension with a resolution that is smaller than the actual mesh width. As becomes evident from Figure 3, the differences between the bubble dimensions in both directions and between the three cases are very small.

At this point it is appropriate to mention some important restrictions of the present concept for simulation of BTF. Due to the use of periodic boundary conditions in axial direction, the length of the unit cell, the axial pressure drop per reference length and the volumetric gas content in the unit cell are input parameters of the simulations, while the gas and liquid flow rates are results, i.e. output. This is in contrast to experiments, where usually the gas and liquid flow rates are specified and the length of the unit cell, the axial pressure drop and the volumetric gas content in the unit cell adjust accordingly. For a comparison with experiments it is therefore important to study the influence of the length of the flow unit cell, L_{uc}. A preliminary respective study for five different values of L_{uc} in the range $1 \leq L_{uc} / L_{ref} \leq 2$ and for the physical parameters mentioned above has been performed by Wörner et al. (2004). Here, this study is continued and refined. Justified by the present results for the influence of the gas properties and the grid size, in all these runs a uniform isotropic grid with a resolution of 48 × 48 mesh cells per channel cross section is used, and the physical properties of the gas phase are set to ρ_G = 11.7 kg/m^3 and $\mu_G = 1.84 \times 10^{-4}$ Pa s. Beside the change of L_{uc} and that of the initial bubble shape from spherical to elongated (see Figure 1 for

the initial bubble shape of case E and Wörner et al. (2004) for its mathematical description) all the other parameters of the simulations including ε and Eu_{ref} are identical to run A2.

2.3. Verification

Table 2 lists the different values of L_{uc} and the corresponding simulation results. These include the bubble velocity U_{B} (which is equal to the mean gas velocity U_{G}), the mean liquid velocity U_{L}, the bubble diameter D_{B}, and the bubble length L_{B}. In all simulations the bubble shape is axisymmetric and, therefore, any axial cross section through the bubble results in a circle. The bubble diameter D_{B} is defined as the largest diameter of this circle for all axial cross sections of the bubble. From Table 2 one can see that with increasing length of the unit cell the bubble velocity and the mean liquid velocity both increase for a given value of Eu_{ref}, respectively $|\Delta p_{L\mathrm{ref}}|$. Thus, for the same gas content within the unit cell and for the same driving axial pressure gradient larger bubble velocities are reached in longer unit cells. The bubble Reynolds number $Re_{\mathrm{B}} \equiv \rho_{\mathrm{L}} W U_{\mathrm{B}} / \mu_{\mathrm{L}}$ is in the range 3.8–4.8, therefore the flow is laminar. Also given in Table 2 are the capillary number Ca and the ratio of bubble velocity to total superficial velocity $V \equiv U_{\mathrm{B}} / J$, where $J \equiv \varepsilon U_{\mathrm{G}} + (1-\varepsilon) U_{\mathrm{L}}$, and the relative bubble velocity $\mathrm{Z} \equiv (U_{\mathrm{B}} - J) / U_{\mathrm{B}}$. The capillary number is proportional to the bubble velocity therefore Ca also increases with increasing length of the unit cell.

For verification we use experimental results of Thulasidas et al. (1995) for D_{B}/W, V and Z, which are given in graphical form as function of the capillary number. Thulasidas et al. (1995) do not give explicit values for the bubble length, but their bubbles are always elongated so that the ratio L_{B}/W is clearly larger than 1. They give, however, values for the ratio of bubble length to unit cell length $L_{\mathrm{B}}/L_{\mathrm{uc}}$, which is in the range 0.6–0.7 and thus is smaller than in our simulations, where it ranges from 0.93 in case A to 0.77 in case H. The experimental values of D_{B}/W, V and Z within the range of Ca of our simulations are listed in the last line of Table 2. We see that the computed values do well agree with the experimental ones with the only exception of cases A1, A2 and A3, where the bubble diameter is clearly too small. The plot of D_{B}/W, V and Z as function of the capillary number in Figure 4 shows that one can identify essentially two regimes with different trends. For cases A, B and C the capillary number is almost the same and we find, for increasing L_{uc}, an increase of D_{B} and a decrease of V and Z. For cases D, E, F, G and H the capillary number increases with increase of L_{uc} because the bubble velocity increases. While the bubble diameter is almost the same in all these cases, V and Z increase with increasing L_{uc} and show a linear increase with Ca. The trends observed in the experiment of Thulasidas et al. (1995), for increasing Ca, are a decrease of D_{B} and an increase of V and Z. Thus, from the present simulations only cases D, E, F, G and H obey this experimental trend for V and Z. We relate these findings to the ratio between bubble length and channel width. For cases A, B and C we have $L_{\mathrm{B}}/W < 1.1$, while for cases D, E, F, G and H and in the experiment of Thulasidas et al. (1995) we have $L_{\mathrm{B}}/W > 1.1$. Our results therefore suggest that bubble-train flow with “short” and “long” bubbles show some different behaviour and the critical value separating both regimes is about $L_{\mathrm{B}}/W \approx 1.1$. We note that for cases D, E, F, G and H the bubble diameter D_{B} is almost independent of Ca whereas the experiments of Thulasidas et al. (1995) show a decrease of D_{B} for increasing values of Ca. For very long bubbles one may expect that for a given value of the capillary number the thickness of the liquid film and therefore D_{B} should become almost independent of the bubble length. However, in the present simulations the bubbles are rather short and the increase of Ca is accompanied by an increase of the bubble length. So we expect a relation $D_{\mathrm{B}} = D_{\mathrm{B}}(Ca, L_{\mathrm{B}})$ instead of $D_{\mathrm{B}} = D_{\mathrm{B}}(Ca)$. Therefore, the expected decrease of D_{B} with increase of Ca for sufficiently long bubbles may, in the present simulations, be counteracted by an increase of D_{B} with increasing bubble length for a given value of Ca.

2.4. Bubble shape and velocity field

Figure 5 shows a visualization of the computed bubble shape and flow field for cases A2, E and H. To allow for a good visualization, the results are shown for each case for an instant in time when the bubble tip is almost at the top of the computational domain. In all simulations the bubble is axisymmetric, i.e. its cross section at any axial position is circular. It is therefore sufficient to display only the left half of the steady bubble shape. Similar visualizations for cases C and G are displayed in Wörner et al. (2005a, 2005b). Figure 5 also shows the velocity field in the vertical axial mid-plane for the three cases. In the left half of the figure the velocity field is shown in the fixed frame of reference, while in the right half it is displayed in the frame of reference moving with the bubble (i.e. the bubble velocity is subtracted from the vertical velocity component). In the fixed frame of reference it can be seen that the velocity profile in the liquid slug has the form of a parabola and is similar for all three cases. In the region where the liquid film is very thin the liquid velocity is almost zero. In the frame of reference moving with the bubble the flow inside the bubble can be analysed. We find that there is one big vortex which occupies almost the complete bubble. In the rear part of the bubble, however, the velocity is almost zero in the moving frame of reference. For the flow in the liquid, the blank regions in the right half of the figures indicate that part of the liquid slug that is moving with the velocity of the bubble.

3. Numerical evaluation of residence time distribution

3.1. Tracking of mass-less particles

We now describe our procedure to evaluate the RTD from the DNS data and start by presenting the method for the reconstruction of the tracer paths. In this context we introduce the following definitions. Let $\mathbf{x}_{\mathrm{p},j}$ be the position vector of particle j in the fixed frame of reference and let $\mathbf{v}(\mathbf{x},t)$ be the velocity field in this frame of reference. Then, the time variation of the position of an infinitesimal small mass-less particle in the fixed frame of reference is given by

$$\frac{\mathrm{d}\mathbf{x}_{\mathrm{p},j}}{\mathrm{d}t} = \mathbf{v}\left(\mathbf{x}_{\mathrm{p},j}(t), t\right) \tag{2}$$

Thus, if the particle position at time t^n is known, the position at time $t^{n+1} = t^n + \Delta t^n$ is given by

$$\mathbf{x}_{\mathrm{p},j}(t^{n+1}) \equiv \mathbf{x}_{\mathrm{p},j}^{n+1} = \mathbf{x}_{\mathrm{p},j}^{n} + \int_{t^n}^{t^{n+1}} \mathbf{v}\left(\mathbf{x}_{\mathrm{p},j}(t), t\right)\mathrm{d}t \tag{3}$$

Using an explicit first order Euler forward integration procedure, one can approximate the above formula as

$$\mathbf{x}_{\mathrm{p},j}^{n+1} = \mathbf{x}_{\mathrm{p},j}^{n} + \Delta t^n \cdot \mathbf{v}(\mathbf{x}_{\mathrm{p},j}^{n}, t^n) \tag{4}$$

The computation of the new position of the tracer particle requires therefore knowledge of the fluid velocity at the actual position of the particle. For the case of bubble-train flow the phases are in relative motion, so that the velocity field in the fixed frame of reference changes in time. However, for periodic fully developed bubble-train flow the bubbles move with constant

speed $\mathbf{U}_B = (0, U_B, 0)^T$ and a steady flow is recovered in the referential linked to the centre of mass of the bubble. Let $\mathbf{z}_{p,j}$ be the position vector of particle j in the frame of reference moving with the bubble and let $\mathbf{w}(\mathbf{x})$ be the *steady* velocity field in this frame of reference. Then, the position vector in the moving frame of reference and the one in the fixed frame of reference are related by

$$\mathbf{z} = \mathbf{x} - (t - t_0)\mathbf{U}_B \tag{5}$$

Here, t_0 is the time for which the two frames of reference coincide. The velocity fields in the moving frame of reference and in the fixed frame of reference are related by

$$\mathbf{w}(\mathbf{z}) = \mathbf{v}(\mathbf{x}, t) - \mathbf{U}_B \tag{6}$$

Thus, in a discrete representation in time and with $t_0 = 0$ we obtain from the last two equations

$$\mathbf{z}_{p,j}^n = \mathbf{x}_{p,j}^n - t^n \mathbf{U}_B \tag{7}$$

and

$$\mathbf{v}(\mathbf{x}_{p,j}^n, t^n) = \mathbf{w}(\mathbf{z}_{p,j}^n) + \mathbf{U}_B \tag{8}$$

Inserting Equation (8) into Equation (4) yields

$$\mathbf{x}_{p,j}^{n+1} = \mathbf{x}_{p,j}^n + \Delta t^n \cdot \left(\mathbf{w}(\mathbf{z}_{p,j}^n) + \mathbf{U}_B \right) \tag{9}$$

Equation (9) and Equation (7) allow us to compute the particle path in the fixed frame of reference from knowing the steady velocity field in the moving frame of reference.

Our DNS computer code uses a regular rectilinear staggered grid, where the components of the velocity vector are defined at the centre of those faces of a mesh cell that are normal to the respective coordinate direction. To determine the velocity at the particle position we perform for each velocity component a linear interpolation, which involves the eight nearest face-centred values of the respective velocity component. The time step width Δt^n for the forward Euler step is determined so that the Courant number, based on the local particle velocity, takes a constant value (here this value is 0.1).

3.2. Initialising the particle positions

Up to now we have discussed only the problem of finding the position of a particle at a certain moment of time assuming that its position at a previous time step is known. In order to compute the RTD we must define the initial positions where the particles are released into the flow. Additionally, we have to define a criterion to decide when a particle has left the domain. Thus, we have to discuss the methods for introducing the numerical tracer and for "measuring" it.

3.2.1. Single phase flow

Levenspiel and Turner (1970) and Levenspiel et al. (1970) point out that there exist two different ways of introducing and measuring tracer. These are the flux introduction and planar

introduction and the flux measurement and planar measurement, respectively. In the flux introduction method the amount of tracer introduced within the cross-section of a duct is proportional to the velocity within this cross-section. Thus, more tracer particles are released in the centre of the duct and less close to the walls, where the velocity is low. Accordingly, the principle of the flux measurement method is to catch all the exit fluid by a "mixing cup measurement". The flux introduction and flux measurement are thus related to the volumetric flow rate entering and leaving the duct within a certain time interval. In contrast, the planar introduction and planar measurement do not rely on a time interval but on a certain instant in time. Therefore, in the planar introduction the tracer is evenly distributed across the cross-section of the duct while the planar measurement detects the instantaneous tracer concentration within the cross-section. The various combinations of the input-output methods give different curves. For reactor purposes, the flux introduction - flux measurement method (flux-flux) is appropriate and gives the proper RTD curve denoted as E. The flux-planar and planar-flux methods both yield the curve E^* while the planar-planar method yields E^{**}.

For comparing different reactors it is useful to introduce an RTD curve $E_\theta \equiv \tau E$, which is measured in terms of the mean residence time $\theta \equiv t / \tau$ (Levenspiel et al., 1970). Here, τ is the mean hydrodynamic residence time, which is defined as the ratio between reactor volume and volumetric flow rate. Similarly, one can define $E_\theta^* \equiv \tau E^*$ and $E_\theta^{**} \equiv \tau E^{**}$. For laminar single-phase flow between two parallel plates, the different curves can be transformed by the relationship (Levenspiel, 1979)

$$E_\theta^{**} = \theta E_\theta^* = \theta^2 E_\theta = \begin{cases} 0 & \text{for} \quad \theta < \theta_{\min} = 2/3 \\ \dfrac{1}{3\theta}\left(1 - \dfrac{2}{3\theta}\right)^{-\frac{1}{2}} & \text{for} \quad \theta \geq \theta_{\min} = 2/3 \end{cases} \tag{10}$$

Note that the mean value of E_θ is identical to τ, while the mean values of E_θ^* and E_θ^{**} are ∞.

The flux-flux method is suitable for a CFD method where the RTD is computed by solving a convection-diffusion equation for the tracer concentration. For a particle method the realisation of the flux-flux method is not straight forward. Therefore, in the present approach we test two procedures. In the first one, which corresponds to the planar introduction, it is essential that the particles are uniformly distributed in the inlet plane. This is ensured by specifying a certain number of particles per reference length, $n_{L\mathrm{ref}}$, which is an input parameter of our method. The distance between neighbouring particles in each coordinate direction is therefore $L_{\mathrm{ref}} / n_{L\mathrm{ref}}$. For a cross-section of size $L_{\mathrm{ref}} \times L_{\mathrm{ref}}$ then $N_{\mathrm{p}} = n_{L\mathrm{ref}} \times n_{L\mathrm{ref}}$ particles are released in the inlet plane, e.g at $y = 0$. The trajectories of all particles are then computed and for each particle the time needed to reach the outlet plane is stored. By classifying the travel time of all particles into certain time intervals of width $\Delta t_{\mathrm{class}}$ a histogram is produced. This histogram is normalized by $N_{\mathrm{p}} \cdot \Delta t_{\mathrm{class}}$. By this procedure we obtain a curve which we denote E_{I}. The second method aims to reproduce the flux introduction and is similar to the first method. However, the residence time of any particle is weighted by the ratio between the local axial velocity at the initial position of the particle and the mean axial velocity in the inlet cross section. We denote the resulting curve as E_{II}.

To test the methods we evaluated the curves $E_{\theta,\mathrm{I}}$ and $E_{\theta,\mathrm{II}}$ from DNS data of laminar single phase flow in a plane channel. The results are shown in Figure 6 for $\Delta\theta_{\mathrm{class}} = 0.047$ (stair-type curves) in double-logarithmic scale and are compared to the analytical results for E_θ, E_θ^* and E_θ^{**} as given by Equation (10). We see that $E_{\theta,\mathrm{I}}$ agrees with E_θ^*, while $E_{\theta,\mathrm{II}}$ agrees with E_θ and

can thus be considered as approximation of the real RTD curve. We also computed the laminar single phase flow in a straight duct with square cross-section and investigated the influence of $n_{L\mathrm{ref}}$ (Wörner et al., 2005a). We found that the mean value of $E_{\theta,\mathrm{I}}$ is 2.87 for $n_{L\mathrm{ref}}$ = 48, is 3.47 for $n_{L\mathrm{ref}}$ = 96, and is 4.13 for $n_{L\mathrm{ref}}$ = 192. These values are clearly larger than the mean hydraulic residence time which corresponds to a mean value of 1. The increase of the mean value of $E_{\theta,\mathrm{I}}$ with increasing number of particles suggests that the mean value will indeed go to infinity for large values of $n_{L\mathrm{ref}}$ as it should for laminar flow.

3.2.2. Two- phase flow

While the particle introduction at the inlet cross-section described above is reasonable to determine the E curve for single phase flow, it can not be used for bubble-train flow. The reason is that releasing particles at a certain instant in time in a cross-section fully occupied by liquid (i.e. a cross-section within the liquid slug) will not be a representative particle subset for the liquid phase. By such a procedure the contributions of the liquid film flow and the corner flow would be missed. Therefore, with exception of two-phase flows which do not show any axial variation of the cross-sectional void distribution (i.e. stratified flow and annular flow), the concept of the particle introduction must be extended.

In this paper we propose an extension of the planar introduction concept from single-phase flow to two-phase flow, namely a *volumetric* introduction. In this volumetric introduction, particles are initially distributed in the entire liquid phase within the unit cell and not only in the inlet cross section. To have a representative sample of particles we adopt the following procedure. The normalisation used in TURBIT-VOF requires $L_\mathrm{z} = L_\mathrm{ref}$, so that the size of the computational domain is $L_\mathrm{x} \times L_\mathrm{uc} \times L_\mathrm{ref}$ and its volume is $L_\mathrm{x} L_\mathrm{uc} L_\mathrm{ref}$. Within this domain in total $n_{L\mathrm{ref}}$ (L_x / L_ref) × $n_{L\mathrm{ref}}$ (L_uc / L_ref) × $n_{L\mathrm{ref}}$ uniformly distributed virtual particles are initialised. Released are, however, only particles which are located inside mesh cells that are entirely filled with liquid (i.e. those mesh cells where f = 1). Thus, mesh cells which contain both liquid and gas are presently ignored. The number of particles for which trajectories are computed is thus approximately

$$N_\mathrm{p} = (1-\varepsilon) n_{L\mathrm{ref}}^3 \frac{L_\mathrm{x} L_\mathrm{uc}}{L_\mathrm{ref}^2} \tag{11}$$

In our DNS simulations the flow is spatially periodic and the periodicity length is equal to the length of the flow unit cell L_uc. It is therefore reasonable to take the required travelling distance of any particle to be a multiple of the length of the flow unit cell

$$L_\mathrm{travel} = n_\mathrm{uc} L_\mathrm{uc} \tag{12}$$

Here, n_uc is a positive integer. In this paper we only consider the case n_uc = 1. Similar to the procedure for single-phase flows described above, we realised two methods for evaluation of the RTD. In the first method, yielding E_I, the travel times of all particles are again equally weighted. In the second method, yielding E_II, the travelling time of any particle is weighted by the ratio between the local axial liquid velocity at the initial position of the particle and the mean liquid axial velocity within the unit cell.

4. Results for the RTD of bubble-train flow

In this section we give results for the RTD curve of the liquid phase in bubble-train flow and only present results for method E_{II} which should correspond to the real RTD with flux introduction and flux measurement. RTD curves obtained by method E_I are given in Wörner et al. (2005a), where they are denoted as V-RTD. In that paper we compared, as a first test, the V-RTD curves obtained from the DNS data of cases A2 and A3, which differ only by the number of grid cells (48^3 and 64^3, respectively). For this comparison we used $n_{L\mathrm{ref}} = 64$ and found that the differences of the curves are very small (see Figure 3 in Wörner et al., 2005a). This is also an indication that the linear interpolation of the discrete velocity field that is used to obtain the particle velocity is sufficiently accurate. In Figure 7 we show the RTD curve (method E_{II}) for case A2 for three different values of $n_{L\mathrm{ref}}$. While the curves are very similar, the one for $n_{L\mathrm{ref}} = 96$ is clearly the smoothest, especially for larger values of t. We found that, in general, the shape of the RTD is more sensitive to the choice of $\Delta t_{\mathrm{class}}$ than to that of $n_{L\mathrm{ref}}$.While small values of $\Delta t_{\mathrm{class}}$ may result in quite different values of E for neighbouring classes, larger values of $\Delta t_{\mathrm{class}}$ lead to smoother curves but have a coarser resolution. Here, we use for Figure 7 and Figure 8 the value $\Delta t_{\mathrm{class}} / t_{\mathrm{ref}} = 0.1$.

The dashed vertical line in Figure 7 is the bubble breakthrough time $t_B \equiv L_{uc} / U_B$. This is the time the bubble needs to move an axial distance equivalent to L_{uc}. From Figure 7 we see that no fluid particles are moving faster than the bubble, a result that is to be expected. However, most of the fluid particles have a residence time that is only slightly larger than t_B. These fluid particles belong to the liquid slug region behind the bubble, which is moving almost with the bubble velocity, as indicated by the velocity profiles in the right half of Figure 5. The long tails in the RTD on the other hand correspond to the flow in the liquid film which is almost stagnant (see velocity profiles in the left half of Figure 5).

The inset graphics in Figure 7 shows the RTD for $n_{L\mathrm{ref}} = 96$ in semi-logarithmic representation. The almost constant slope indicates that the curve may well be approximated by an exponential relationship. This and the above discussion for the bubble breakthrough time suggest that the RTD curve in Figure 7 may be approximated by a compartment model for single-phase flow which consists of two "tanks" in series. The first tank is a plug flow reactor and the second tank is a continuous stirred tank reactor which is perfectly mixed (see Figure 12.1 in Levenspiel, 1999). This concept has already been adopted by Salman et al. (2004) to develop an analytical model for predicting axial mixing during Taylor flow in microchannels at high Bodenstein numbers. The RTD of this compartment model is given by (Levenspiel, 1999)

$$E = \begin{cases} 0 & \text{for } t < V_{\mathrm{PFR}} / Q \\ \dfrac{Q}{V_{\mathrm{CSTR}}} \exp\left(-\dfrac{Q}{V_{\mathrm{CSTR}}} \cdot t + \dfrac{V_{\mathrm{PFR}}}{V_{\mathrm{CSTR}}} \right) & \text{for } t \geq V_{\mathrm{PFR}} / Q \end{cases} \tag{13}$$

where Q is the volumetric flow rate of the single-phase flow and V_{PFR} and V_{CSTR} are the volumes of the plug flow reactor and the continuous stirred tank reactor, respectively. The ratio V_{PFR} / Q defines the "delay time" necessary to cross the plug flow reactor. In the case of bubble-train flow this delay time is given by the bubble breakthrough time. We therefore replace in Equation (13) expression V_{PFR} / Q by $t_B = L_{uc} / U_B$. The pre-factor Q / V_{CSTR} in Eq. (13) is associated with the continuous stirred tank reactor, since it is just the inverse of the mean hydrodynamic residence time of the CSTR. For our bubble-train flow, the CSTR corresponds to the liquid slug region, which is well mixed because of the fluids re-circulating

motion (Thulasidas et al., 1997). The liquid slug is moving with the total superficial velocity J. Considering the length of a unit cell, the mean residence time of the liquid slug is therefore given by L_{uc} / J. Replacing in Equation (13) Q / V_{CSTR} by J / L_{uc} yields the following model:

$$E_J = \begin{cases} 0 & \text{for } t < L_{uc}/U_B \\ \dfrac{J}{L_{uc}} \exp\left[\dfrac{J}{L_{uc}} \left(\dfrac{L_{uc}}{U_B} - t \right) \right] & \text{for } t \geq L_{uc}/U_B \end{cases} \tag{14}$$

A variant of the model is obtained when the total superficial velocity J in Equation (14) is replaced by the mean liquid velocity U_L:

$$E_{UL} = \begin{cases} 0 & \text{for } t < L_{uc}/U_B \\ \dfrac{U_L}{L_{uc}} \exp\left[\dfrac{U_L}{L_{uc}} \left(\dfrac{L_{uc}}{U_B} - t \right) \right] & \text{for } t \geq L_{uc}/U_B \end{cases} \tag{15}$$

We note that the above models differ from the analytical model of Salman et al. (2004) in so far as the latter authors approximate V_{PFR} / Q by L_B/U_B and Q / V_{CSTR} by $U_B A_{film} / V_{slug}$, where A_{film} is the cross-sectional area of the liquid film and V_{slug} is the volume of the liquid slug. This model, subsequently called E_{circ}, was developed for circular channels, where the film thickness is uniform and A_{film} can be directly computed from correlations that relate the liquid film thickness to the capillary number. For non-circular channels, however, the film thickness is not uniform and in square channels, for example, there exists considerable corner flow. Nevertheless, for comparison we also present results for model E_{circ}, where we use the approximations $A_{film} \approx W^2 - \pi D_B^2/4$ and $V_{slug} \approx W^2 (L_{uc} - L_B)$.

In Figure 8 we compare the models E_J, E_{UL} and E_{circ} with the evaluated RTD curves (method E_{II}) for case E and H. In this figure the RTD data are represented by the shaded area and are displayed as linear plot and in the inset graphics as semi-logarithmic plot. In the semi-logarithmic plots one can recognize that for $t/t_{ref} > 4$ the RTD changes its slope. The steeper slope for values $t/t_{ref} < 4$ is better fitted by model E_J, whereas the flatter slope for times $t/t_{ref} > 4$ is better approximated by model E_{UL}. This behaviour is reasonable because residence times $t/t_{ref} < 4$ correspond to virtual particles in the liquid slug, which is moving with velocity J, while residence times $t/t_{ref} > 4$ correspond to the flow in the four corners where on average the liquid does not move with the total superficial velocity J but with the lower mean liquid velocity U_L or the even lower liquid superficial velocity $J_L \equiv (1-\varepsilon)\, U_L$. The residence time distribution predicted by the model of Salman et al. (2004) for circular channels, E_{circ}, is too narrow and is not a good approximation of the RTD for square channels. This poor performance of model E_{circ} for square channels may hold at least for capillary numbers $Ca > 0.04$, where the bubble is axisymmetric (Thulasidas et al., 1995) and considerable corner flow exists.

While model E_J can be considered to be already a reasonable approximation for the liquid phase residence time distribution of bubble-train flow in a square channel, the different slopes for small and large times suggest that the model may be further improved by a three tank compartment model. The first tank is, as before, the plug flow reactor which is in series with two parallel continuous stirred tank reactors. One CSTR corresponds, as before, to the liquid slug, while the second corresponds to the liquid corner flow. The RTD of this refined compartment model obeys in a semi-logarithmic representation a superposition of two slopes (see Figure 12.1 in Levenspiel, 1999), as it is observed in Figure 8.

5. Conclusions and outlook

In this paper we presented an original method for evaluating the liquid phase residence time distribution of bubble-train flow using data from direct numerical simulations. The method is a particle method and relies on the uniform introduction of virtual particles in the volume occupied by the liquid phase within a single flow unit cell. The residence time distribution is obtained by statistical evaluation of the time needed by virtual particles to travel an axial distance equivalent to the length of the unit cell, and by an appropriate weighting procedure which takes into account the axial velocity at the particles initial position. Residence time curves have been evaluated from DNS data of bubble-train flow in a square mini-channel for different lengths of the flow unit cell, where the capillary number is in the range 0.2–0.25. The RTD curves obtained can well be fitted by a simple exponential relationship, which has been developed on the basis of a compartment model consisting of two tanks in series, the first tank being a plug flow reactor and the second being a continuous stirred tank reactor. This model may also be applicable for bubble-train flow in channels with circular cross-section, where, unlike in channels with rectangular cross section, no corner flow exists and for which the usefulness of a similar model (Salman et al., 2004) has already been demonstrated. For channels with square or rectangular cross-section an extension of the basic model E_J is proposed, which may allow for taking into account corner flow in more detail. This topic will be addressed in future. Also the influence of the capillary number on the residence time distribution and model performance will be investigated.

Up to now we have considered only the RTD for a single unit cell. Unfortunately, we can not compare our RTD model with experimental data, because measurements of the RTD for a single unit cell are not available. In practice, a duct with bubble-train flow will contain tens or hundreds of unit cells. We will therefore apply our method to multiple lengths of the unit cell (n_{uc} = 2,3, …) and determine the respective RTD curves. In particular, it will be interesting to check if the RTD for an arbitrary number of n_{uc} can be obtained by convolution of the RTD for a single flow unit cell (n_{uc} = 1). In this case, the developed model E_J will be very useful since the determination of the RTD of bubble-train flow will require only information about the total superficial velocity and the bubble velocity. Then, it will also be possible to validate the model by comparison with measured RTD curves (e.g. Thulasidas et al. 1999; A. Günther et al. 2004; Trachsel et al. 2005).

An interesting result of the direct numerical simulations of bubble-train flow in a square mini-channel for various values of the unit cell length are the different trends observed for the dependence of the bubble diameter, the ratio of bubble velocity to total superficial velocity and of the non-dimensional relative bubble velocity on the capillary number for “short” and “long” bubbles. The present results suggest that a criterion for the transition between both regimes may be given by a critical ratio of bubble length to channel width of about 1.1. To the authors’ knowledge, this topic has not been investigated up to now and deserves further studies.

References

Boger, T., Heibel, A.K., Sorensen, C.M., 2004. Monolithic catalysts for the chemical industry. Ind. Eng. Chem. Res. 43, 4602–4611.

Burns, J.R., Ramshaw, C., 2001. The intensification of rapid reactions in multiphase systems using slug flow in capillaries. Lab Chip 1, 10–15.

Castelain, C., Berger, D., Legentilhomme, P., Mokrani, A., Peerhossaini, H., 2000. Experimental and numerical characterisation of mixing in a steady spatially chaotic flow by means of residence time distribution measurements. Int. J. Heat Mass Tran. 43, 3687–3700.

Ghidersa, B., Wörner, M., Cacuci, D.G., 2004. Exploring the flow of immiscible fluids in a square vertical mini-channel by direct numerical simulation. Chem. Eng. J. 101, 285–294.

Günther, A., Khan, S.A., Thalmann, M., Trachsel, F., Jensen, K.F., 2004. Transport and reaction in microscale segmented gas-liquid flow. Lab Chip 4, 278–286.

Günther, M., Schneider, S., Wagner, J., Gorges, R., Henkel, T., Kielpinski, M., Albert, J., Bierbaum R., Köhler, J.M., 2004. Characterisation of residence time and residence time distribution in chip reactors with modular arrangements by integrated optical detection. Chem. Eng. J. 101, 373–378.

Heibel, A.K., Lebens, P.J.M., Middelhoff, J.W., Kapteijn, F., Moulijn, J., 2005. Liquid residence time distribution in the film flow monolith reactor. AICHE J. 51, 122–133.

Hessel, V., Hardt, S., Löwe, H., 2004. Chemical micro process engineering. Wiley, Weinheim.

Hessel, V., Angeli, P., Gavriilidis, A., Löwe, H., 2005. Gas-liquid and gas-liquid-solid microstructured reactors: contacting principles and applications. Ind. Eng. Chem. Res. 44, 9750–9769.

Kreutzer, M.T., Bakker, J.J.W., Kapteijn, F., Moulijn, J.A., Verheijen, P.J.T., 2005a. Scaling-up multiphase monolith reactors: linking residence time distribution and feed maldistribution. Ind. Eng. Chem. Res. 44, 4898–4913.

Kreutzer, M.T., Kapteijn, F., Moulijn J.A., Ebrahimi, S., Kleerebezem, R., van Loosdrecht, M.C.M, 2005b. Monoliths as biocatalytic reactors: smart gas-liquid contacting for process intensification. Ind. Eng. Chem. Res. 44, 9646–9652.

Levenspiel, O., 1979. The chemical reactor omnibook. OSU Book stores Inc., Corvallis, OR.

Levenspiel, O., 1999. Chemical Reaction Engineering. 3rd ed., Wiley, New York.

Levenspiel, O., Turner, J.C.R., 1970. The interpretation of residence-time experiments. Chem. Eng. Sci. 25, 1605–1609.

Levenspiel, O., Lai, B.W., Chatlynne, C.Y., 1970. Tracer curves and the residence-time distribution. Chem. Eng. Sci. 25, 1611–1613.

Nauman, E.B., 1981. Residence time distributions and micromixing. Chem. Eng. Commun. 8, 53–131.

Patrick, R.H. Jr., Klindera, T., Crynes L.L., Cerro, R.L., Abraham, M.A., 1995. Residence time distribution in three-phase monolith reactor. AIChE J. 41, 649–657.

Sabisch, W., Wörner, M., Grötzbach, G., Cacuci, D.G., 2001. 3D volume-of-fluid simulation of a wobbling bubble in a gas-liquid system of low Morton number. In: Proc. 4th Int. Conf. Multiphase Flow, New Orleans, USA, May 27 – June 1, 2001.

Salman, W., Gavriilidis, A., Angeli, P., 2004. A model for predicting axial mixing during gas-liquid Taylor flow in microchannels at low Bodenstein numbers. Chem. Eng. J. 101, 391–396.

Salman, W., Angeli, P., Gavriilidis, A., 2005. Sample pulse broadening in Taylor flow microchannels for screening applications. Chem. Eng. Technol. 28, 509–514.

Taha, T., Cui, Z.F., 2006. CFD modelling of slug flow inside square capillaries. Chem. Eng. Sci. 61, 665–675.

Thulasidas, T.C., Abraham, M.A., Cerro, R.L., 1995. Bubble-train flow in capillaries of circular and square cross section. Chem. Eng. Sci. 50, 183–199.

Thulasidas, T.C., Abraham, M.A., Cerro, R.L., 1997. Flow patterns in liquid slugs during bubble-train flow inside capillaries. Chem. Eng. Sci. 52, 2947–2962.

Thulasidas, T.C., Abraham, M.A., Cerro, R.L., 1999. Dispersion during bubble-train flow in capillaries. Chem. Eng. Sci. 54, 61–76.

Thyn, J., Zitny, R., 2004. Radiotracer applications for the analysis of complex flow structure in industrial apparatuses. Nucl. Instrum. Meth. B 213, 339–347.

Trachsel F., Günther, A., Khan, S., Jensen, K.F., 2005. Measurement of residence time distribution in microfluidic systems. Chem. Eng. Sci. 60, 5729–5737.

Wörner, M., Ghidersa, B., Shahab, A.F., 2004. Numerical study of bubble-train flow in a square vertical mini-channel: influence of length of the flow unit cell. In: Proc. 5th Int. Conf. Multiphase Flow, Yokohama, Japan, May 30–June 4, 2004.

Wörner, M., Ghidersa, B., Onea, A., 2005a. Evaluation of residence time distribution for bubble-train flow in a square mini-channel by direct numerical simulation. In: Proc. ECI Int. Conf. Heat Transfer Fluid Flow Microscale, Castelvecchio, Italy, September 25–30, 2005.

Wörner, M., Ghidersa, B., Ilić, M., Cacuci, D.G., 2005b. Volume-of-fluid method based numerical simulations of gas-liquid two-phase flow in confined geometries. La Houille Blanche n°6–2005, 91–104.

Yawalkar, A.A., Sood, R., Kreutzer, M.T., Kapteijn, F., Moulijn, J.A., 2005. Axial mixing in monolith reactors: effect of channel size. Ind. Eng. Chem. Res. 44, 2046–2057.

Nomenclature

Bo	Bodenstein number
Ca	Capillary number
D_{B}	Bubble diameter
E	Residence time distribution (RTD)
Eu_{ref}	Reference Euler number, $Eu_{\mathrm{ref}} = \mid \Delta p_{L\mathrm{ref}} \mid /(\rho_{\mathrm{L}} U_{\mathrm{ref}}^2)$
F	Cumulative residence time distribution function
f	Liquid volumetric fraction in a mesh cell
J_{G}	Superficial velocity of gas phase, $J_{\mathrm{G}} = \varepsilon U_{\mathrm{G}}$
J_{L}	Superficial velocity of liquid phase $J_{\mathrm{L}} = (1-\varepsilon) U_{\mathrm{L}}$
J	Total superficial velocity, $J = J_{\mathrm{G}} + J_{\mathrm{L}}$
L_{B}	Bubble length
L_{ref}	Reference length scale, $L_{\mathrm{ref}} = W = 0.002\,\mathrm{m}$
L_{uc}	Length of unit cell
N_{p}	Number of particles
N_{t}	Number of time steps
$n_{L\mathrm{ref}}$	Number of particles per reference length
$\Delta p_{L\mathrm{ref}}$	Axial pressure drop per reference length
Q	Volumetric flow rate
Re_{B}	Bubble Reynolds number
t	Time
t_{B}	Bubble breakthrough time, $t_{\mathrm{B}} \equiv L_{\mathrm{ref}} / U_{\mathrm{B}}$
U_{B}	Bubble velocity
U_{G}	Mean velocity of gas phase, here $U_{\mathrm{G}} = U_{\mathrm{B}}$
U_{L}	Mean velocity of liquid phase
U_{ref}	Reference velocity scale, $U_{\mathrm{ref}} = 0.0264\,\mathrm{m/s}$
V	Ratio between bubble velocity and superficial velocity, $V \equiv U_{\mathrm{B}} / J$
$V_{\mathrm{PFR}}, V_{\mathrm{CSTR}}$	Volume of reactor
$\mathbf{v}$	Velocity field in fixed frame of reference
W	Channel width, $W = 0.002\,\mathrm{m}$
$\mathbf{w}$	Velocity field in frame of reference moving with the bubble
$\mathbf{x} = (x, y, z)^{\mathrm{T}}$	Cartesian position vector in fixed frame of reference
Z	Non-dimensional relative bubble velocity, $Z \equiv (U_{\mathrm{B}} - J) / U_{\mathrm{B}}$
$\mathbf{z}$	Cartesian position vector in frame of reference moving with bubble

Greek symbols

ε	Volume fraction of gas in the unit cell
μ	Dynamic viscosity
θ	Dimensionless time, $\theta \equiv t/\tau$
ρ	Density
σ	Coefficient of surface tension
τ	Mean hydrodynamic residence time

Subscripts

B	Bubble
CSTR	Continuous stirred tank reactor
G	Gas phase
L	Liquid phase
PFR	Plug flow reactor
ref	Reference value
uc	Unit cell

Tables

Table 1: Parameters of simulations performed to investigate the influence of gas physical properties and grid size for a cubic unit cell ($L_{uc} = W$)

Case	ρ_G [kg/m^3]	μ_G [mPa s]	grid	$\Delta t / t_{ref}$	N_t	t_{max} / t_{ref}
A1	1.17	0.0184	48×48×48	2.5×10^{-6}	300,000	0.75
A2	11.7	0.184	48×48×48	2.5×10^{-5}	40,000	1.0
A3	11.7	0.184	64×64×64	1×10^{-5}	100,000	1.0

Table 2: Results for simulations with different unit cell length

Case	L_{uc}/W	Grid	U_B/U_{ref}	U_L/U_{ref}	Ca	D_B/W	L_B/W	V	Z
A1	1.0	48×48×48	3.66	1.21	0.209	0.811	0.928	1.808	0.447
A2	1.0	48×48×48	3.66	1.20	0.209	0.809	0.934	1.815	0.449
A3	1.0	64×64×64	3.64	1.20	0.208	0.810	0.935	1.812	0.448
B	1.125	48×54×48	3.61	1.26	0.206	0.831	0.993	1.770	0.435
C	1.25	48×60×48	3.62	1.29	0.207	0.842	1.054	1.756	0.430
D	1.375	48×66×48	3.76	1.33	0.215	0.847	1.138	1.755	0.430
E	1.5	48×72×48	3.86	1.37	0.220	0.845	1.208	1.761	0.432
F	1.625	48×78×48	4.10	1.41	0.234	0.849	1.301	1.778	0.437
G	1.75	48×84×48	4.20	1.44	0.240	0.850	1.370	1.786	0.440
H	2.0	48×96×48	4.54	1.51	0.259	0.848	1.533	1.809	0.447
					Experimental data of Thulasidas et al. (1995)				
					0.21–0.26	0.82–0.86	–	1.68–1.84	0.435–0.475

Figures

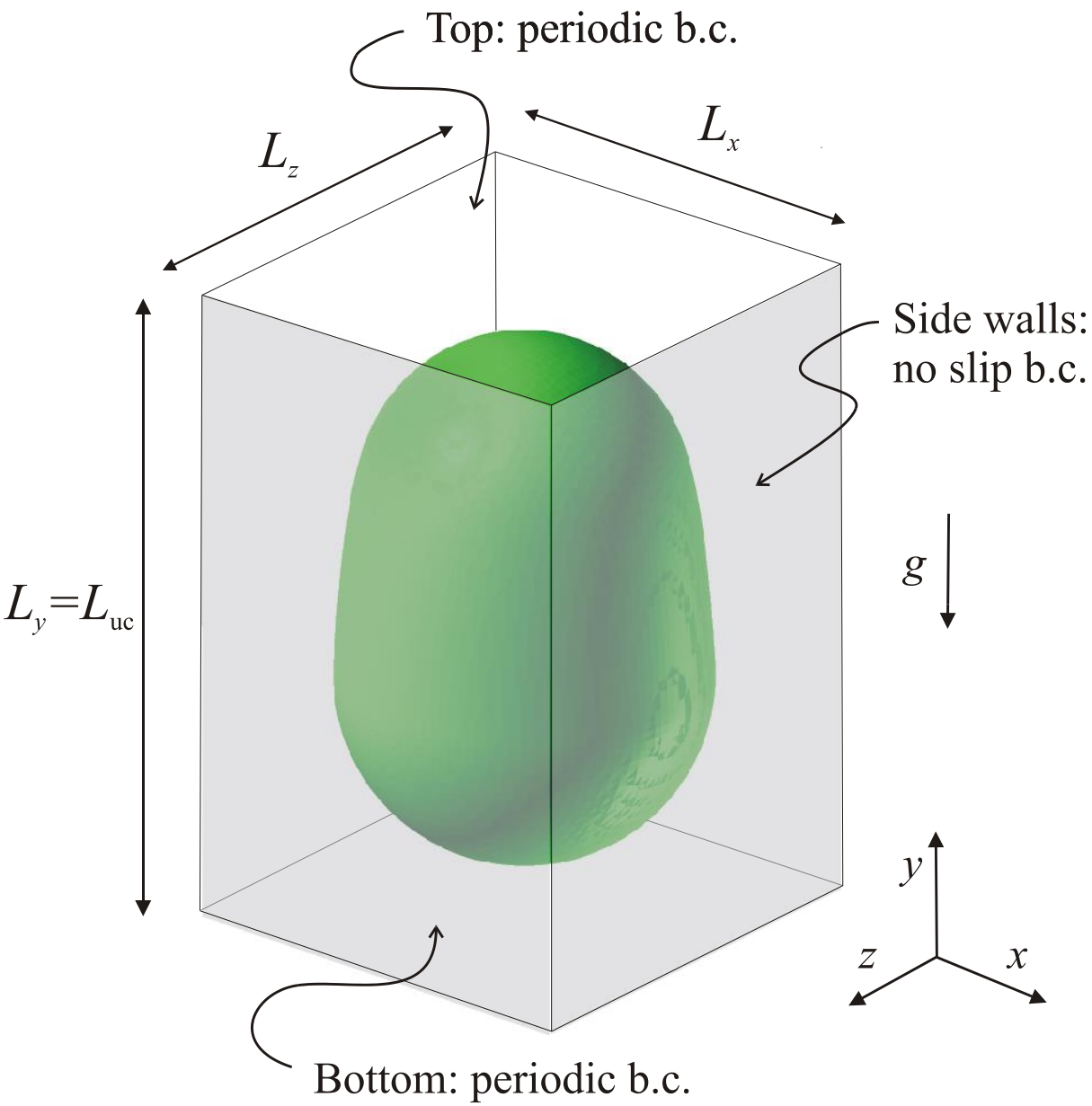

Figure 1: Sketch of computational domain and co-ordinate system. The bubble shape corresponds to the initial conditions of case E.

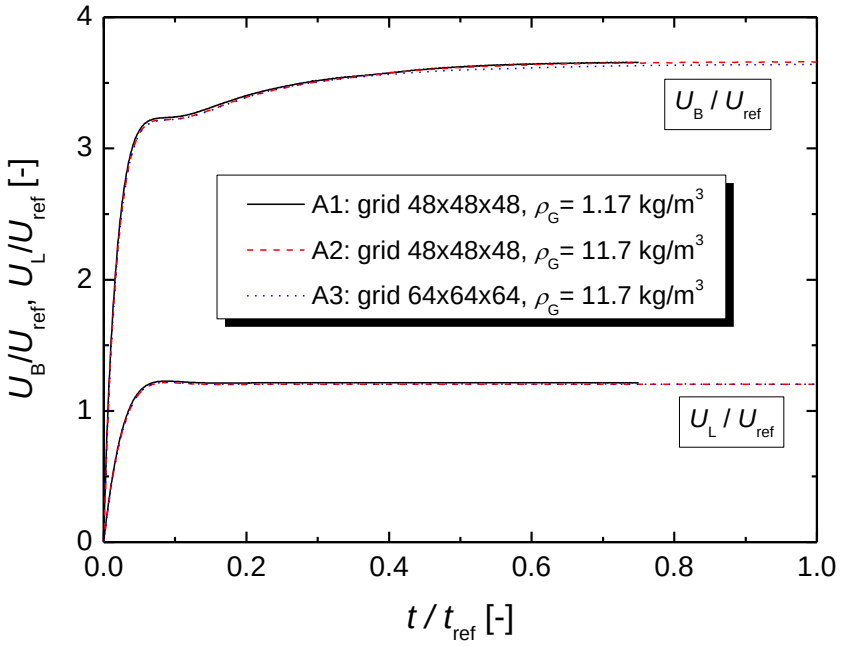

Figure 2: Temporal evolution of non-dimensional bubble velocity and mean liquid velocity for cases A1, A2 and A3.

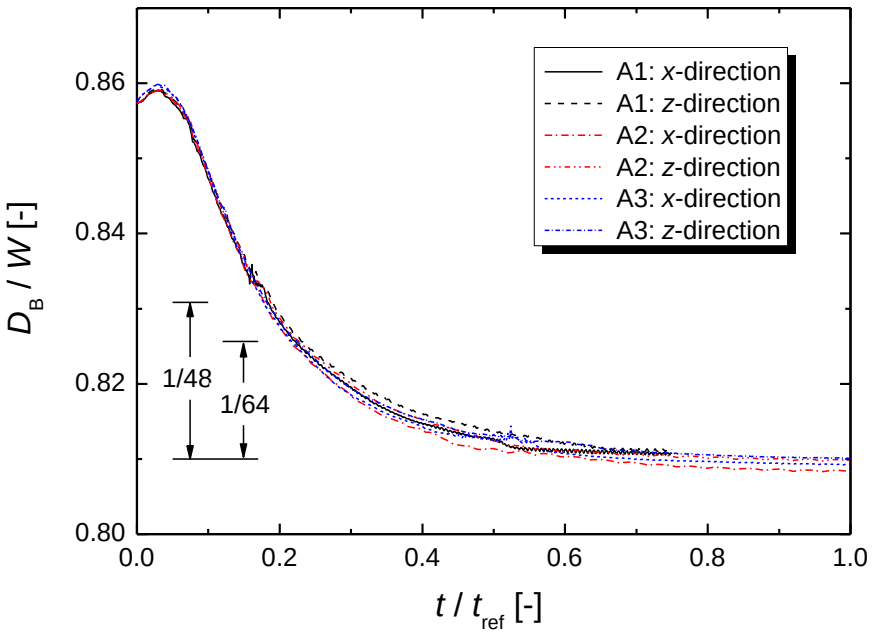

Figure 3: Temporal evolution of non-dimensional bubble dimensions in wall normal directions *x* and *z* for cases A1, A2 and A3. The arrows indicate the mesh cell size for cases A1 and A2 (1/48) and A3 (1/64).

(a)

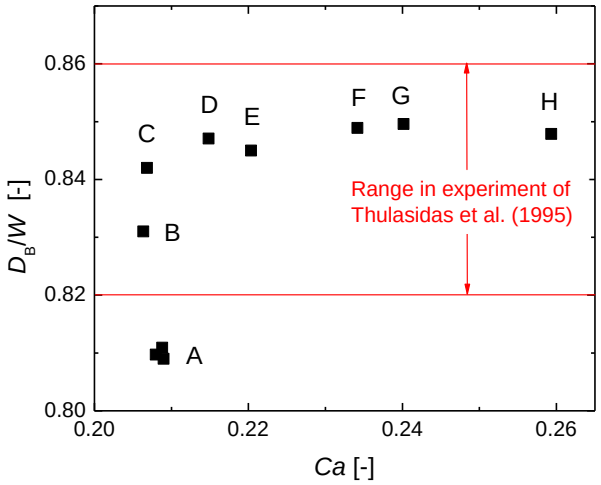

(b)

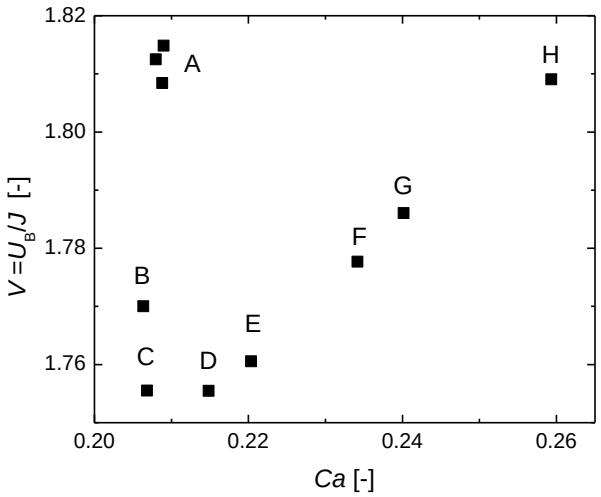

(c)

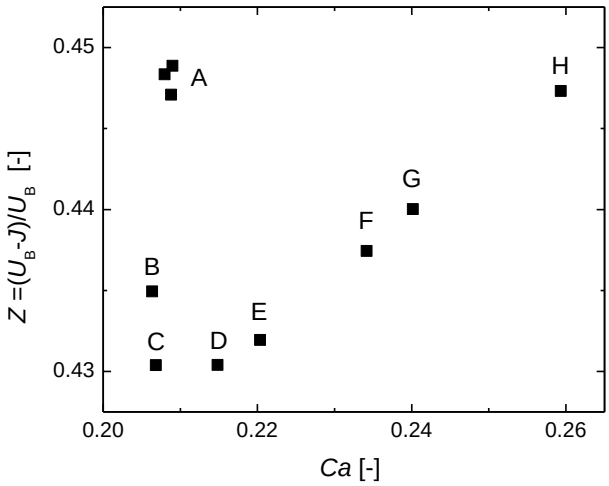

Figure 4: Simulation results for different values of L_{uc} as function of the capillary number: (a) Non-dimensional bubble diameter, (b) ratio of bubble velocity and total superficial velocity, (c) ratio of relative velocity to bubble velocity.

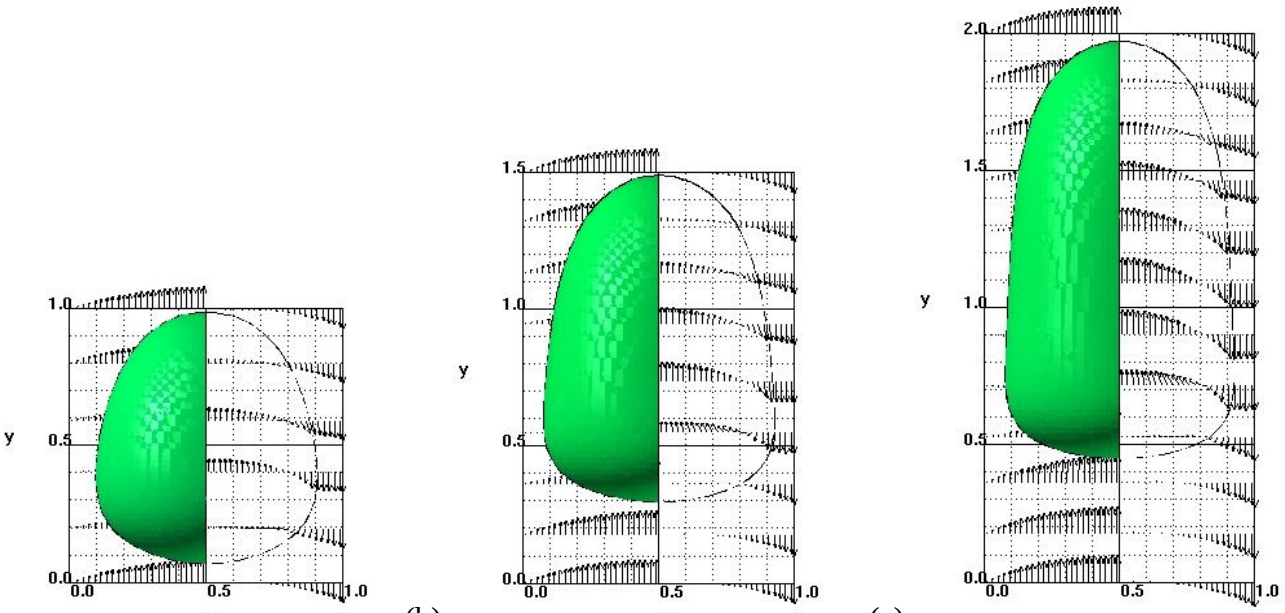

Figure 5: Bubble shape and velocity field in vertical mid-plane z = 1 mm for fixed frame of reference (left half) and for frame of reference linked to the bubble (right half) for (a): case A2, t/t_{ref} = 0.595, (b): case E, t/t_{ref} = 0.44, (c): case H, t/t_{ref} = 0.54. In y-direction only every 8th vector is displayed. Note that the values at the axes correspond to x/L_{ref} any y/L_{ref}.

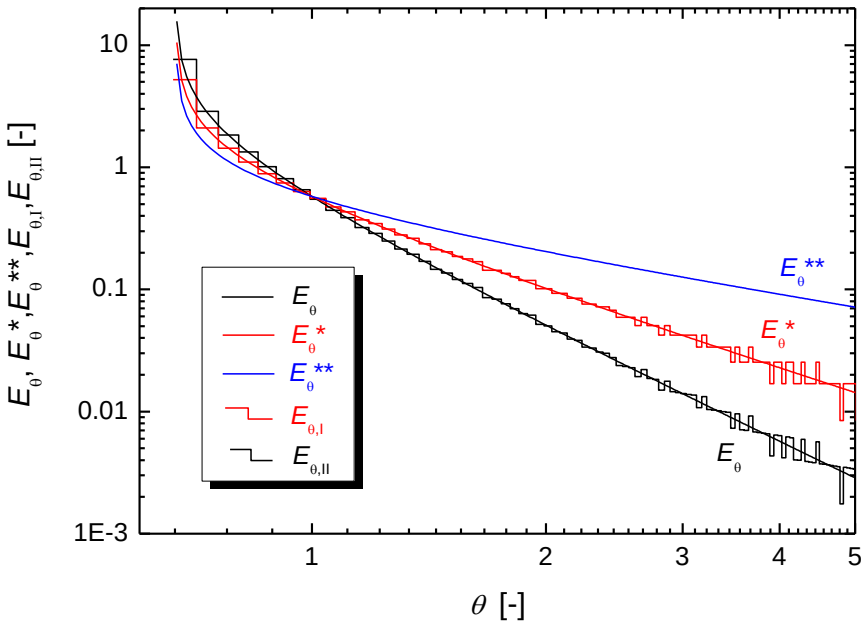

Figure 6: Comparison of RTD curves evaluated by method I and method II with analytical RTD curves for laminar single phase flow in a plane channel.

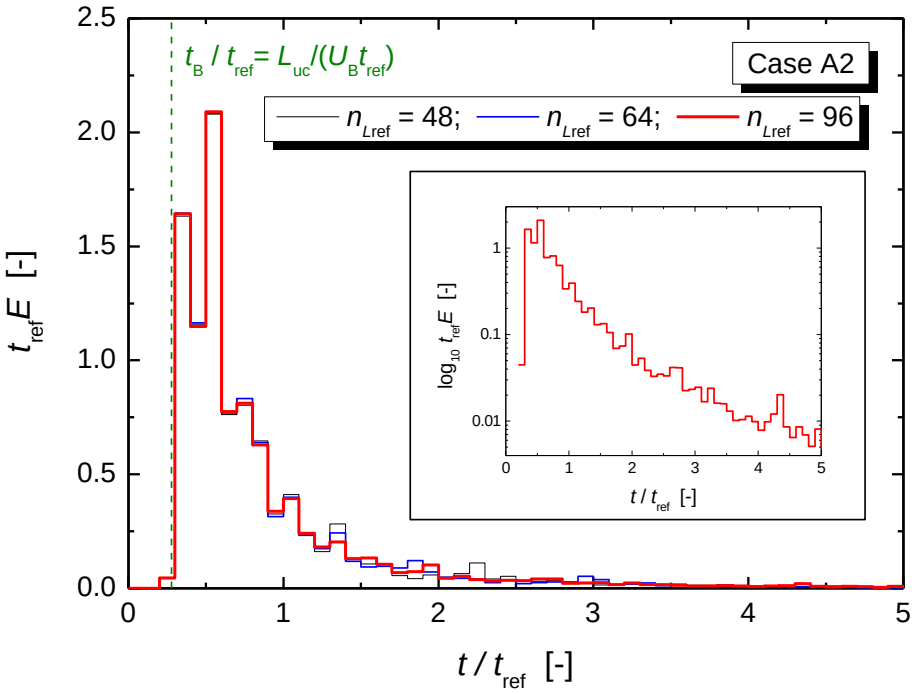

Figure 7: Evaluated RTD curves for the bubble-train flow of case A2 for three different values of n_{Lref}. The dashed vertical line corresponds to the bubble breakthrough time.

(a)

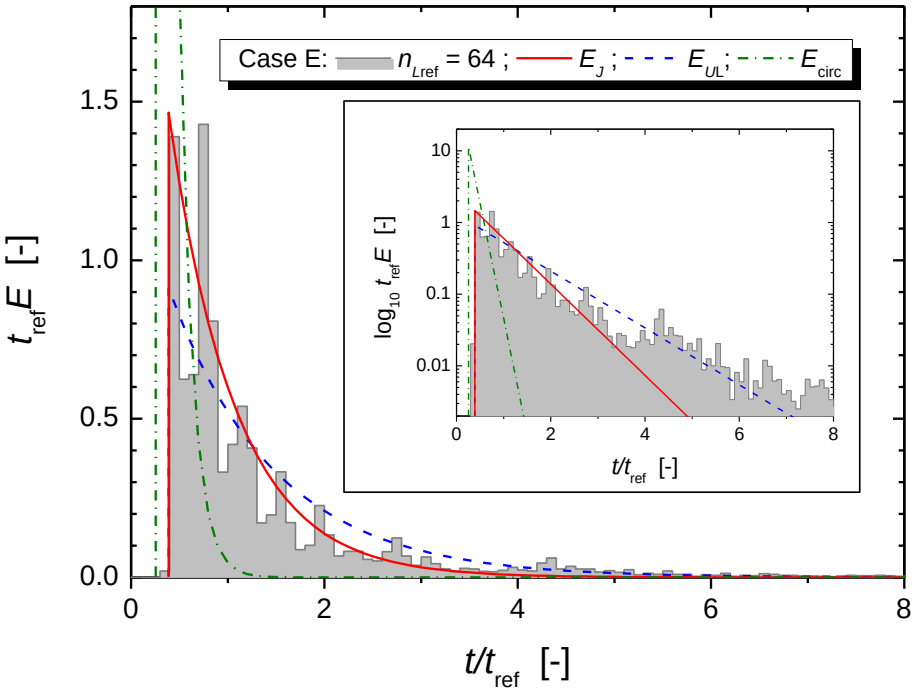

(b)

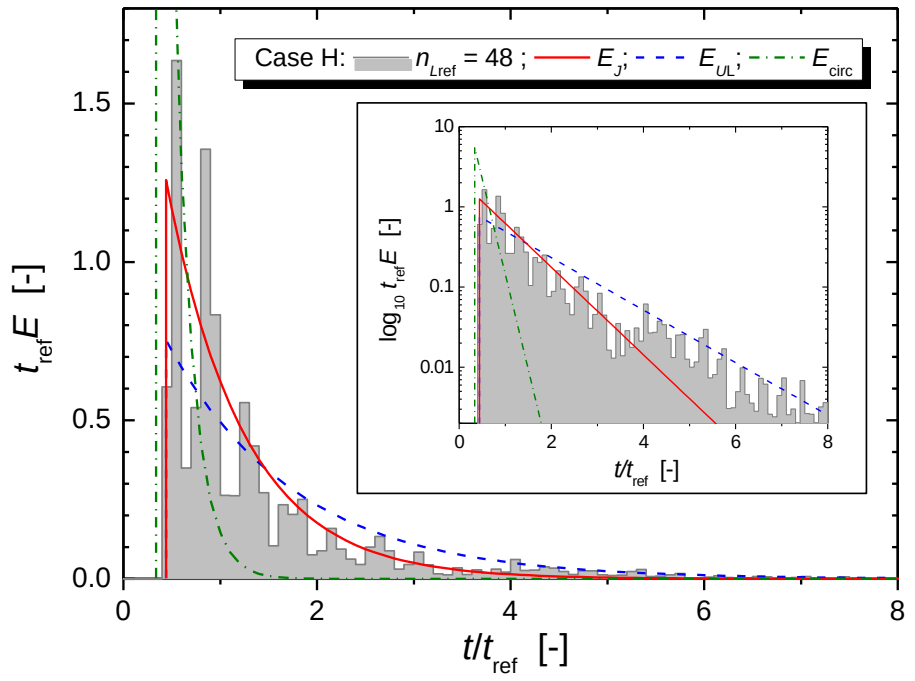

Figure 8: Comparison of evaluated RTD curve of bubble-train flow (shaded area) for case E (a) and H (b) with models E_J , E_{UL} and E_{circ}.